nature energy

SUPPLEMENTARY INFORMATION

DOI: 10.1038/s41560-017-0014-y

In the format provided by the authors and unedited.

High-performance sodium–organic battery by realizing four-sodium storage in disodium rhodizonate

Minah Lee[1], Jihyun Hong[2,3], Jeffrey Lopez[1], Yongming Sun[2], Dawei Feng[1], Kipil Lim[2,3], William C. Chueh[2], Michael F. Toney[3], Yi Cui[2]* and Zhenan Bao[1]*

[1]Department of Chemical Engineering, Stanford University, Stanford, CA 94305, USA. [2]Department of Materials Science and Engineering, Stanford University, Stanford, CA 94305, USA. [3]Stanford Synchrotron Radiation Lightsource, SLAC National Accelerator Laboratory, Menlo Park, CA 94025, USA. *e-mail: yicui@stanford.edu; zbao@stanford.edu

Supplementary information

High performance sodium-organic battery by realizing four-sodium storage in disodium rhodizonate

Minah Lee[1], Jihyun Hong[2,3], Jeffrey Lopez[1], Yongming Sun[2], Dawei Feng[1], Kipil Lim[2,3], William C. Chueh[2], Michael F. Toney[3], Yi Cui[2]*, and Zhenan Bao[1]*

[1]Department of Chemical Engineering, Stanford University, CA 94305, United States
[2]Department of Materials Science and Engineering, Stanford University, CA 94305, United States
[3]Stanford Synchrotron Radiation Lightsource, SLAC National Accelerator Laboratory, Menlo Park, California 94025, United States

Supplementary Figures

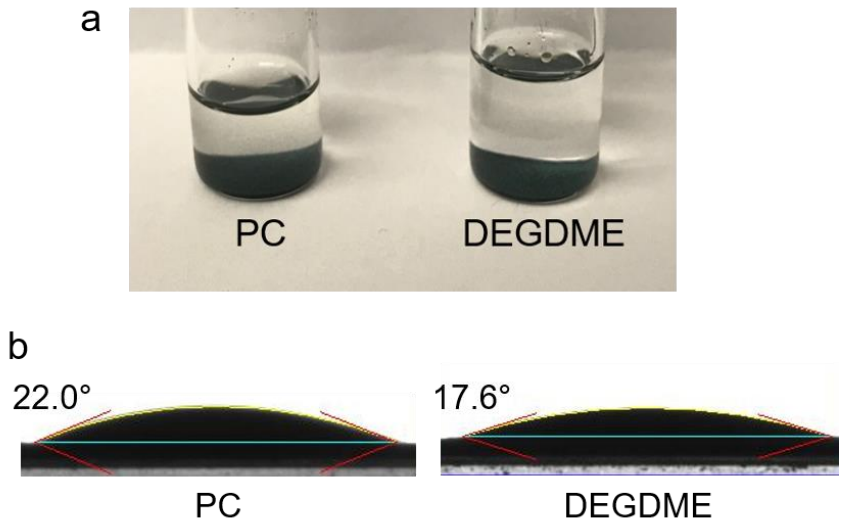

Supplementary Figure 1. a, Solubility test of $Na_2C_6O_6$ in organic electrolytes. There was no sign of dissolution (i.e., color change) after immersing $Na_2C_6O_6$ powder in each electrolyte for seven days. **b,** PC and DEGDME electrolytes exhibit low contact angles of 22.0° and 17.7°, respectively, on $Na_2C_6O_6$ electrode surfaces, confirming good electrolyte wettability for both cases.

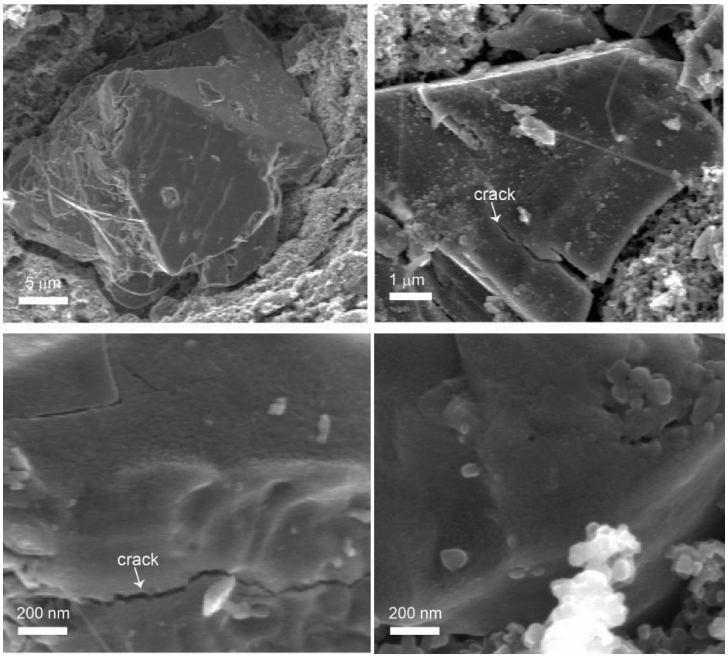

Supplementary Figure 2. SEM images of bulk particles electrodes after cycling.

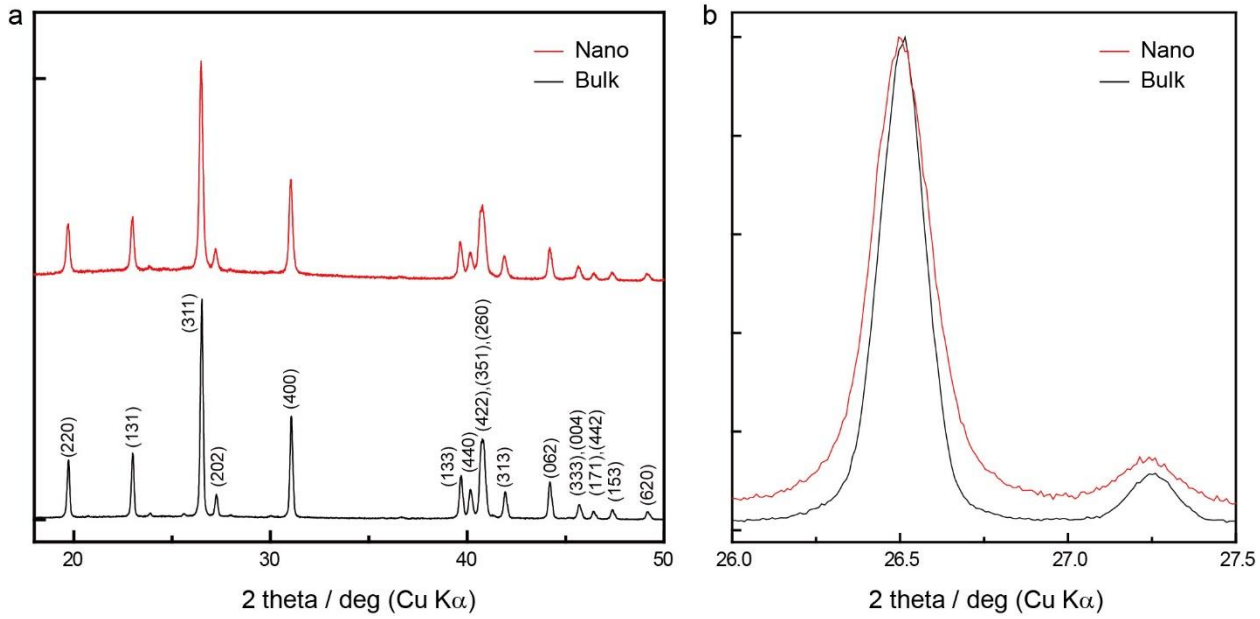

Supplementary Figure 3. a, XRD patterns of $Na_2C_6O_6$ nanoparticles compared with that of bulk particles. **b**, enlarged peaks at 26.5 of XRD patterns.

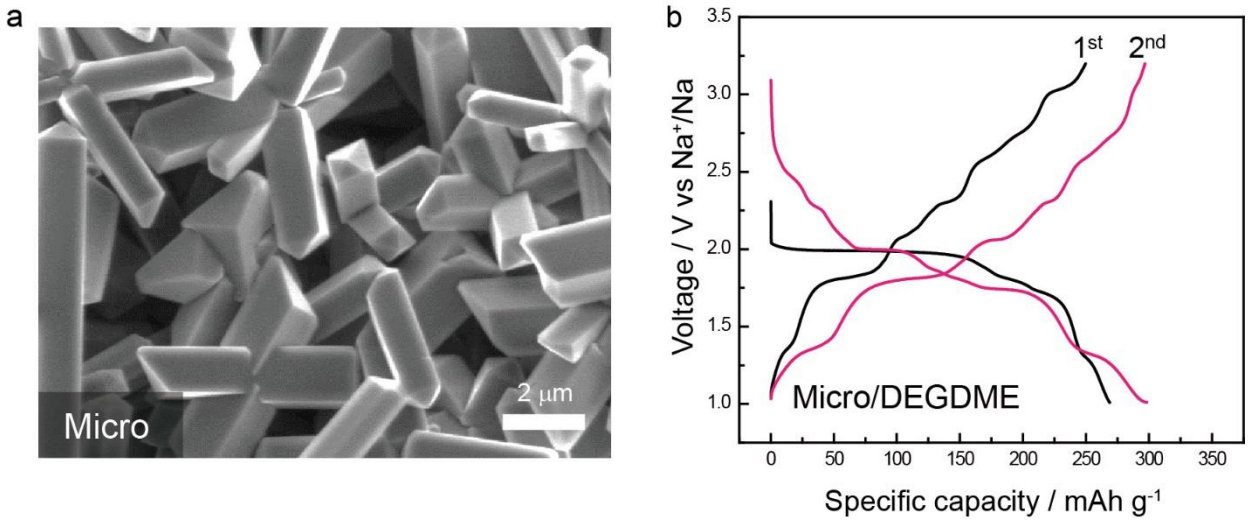

Supplementary Figure 4. a, SEM image of $Na_2C_6O_6$ particles on the order of several micrometers (Micro). **b**, First and second discharge/charge cycles of $Na_2C_6O_6$ Micro electrodes in DEGDME from a potential window of 1.0-3.2 V. The capacity was slightly increased by 26 mAh g^{-1} in the second cycle compared to the first cycle. The total discharge capacity in the second cycle was 299 mAh g^{-1} which is higher than that of Bulk and lower than that of Nano. The plateau at 2.0 V of the initial discharge was partially maintained in the second discharge. The separate discharge capacity from this plateau region was 73 mAh g^{-1}, which is also in between that of Bulk (52 mAh g^{-1}), and Nano (94 mAh g^{-1}).

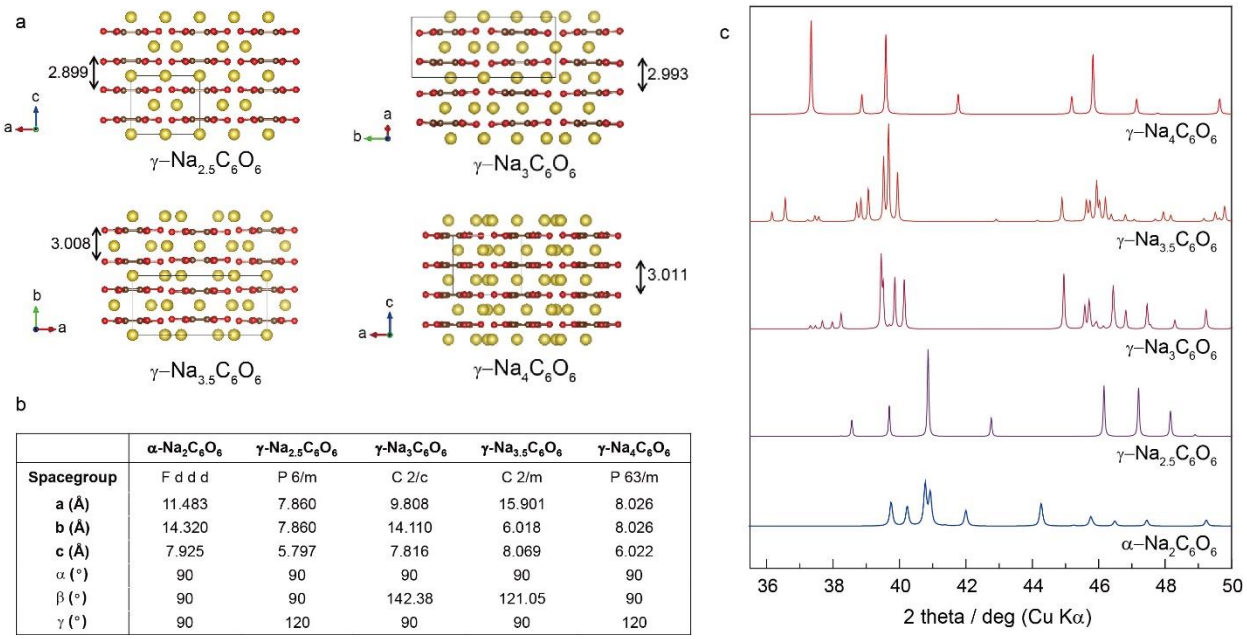

b

	α-$Na_2C_6O_6$	γ-$Na_{2.5}C_6O_6$	γ-$Na_3C_6O_6$	γ-$Na_{3.5}C_6O_6$	γ-$Na_4C_6O_6$
Spacegroup	F d d d	P 6/m	C 2/c	C 2/m	P 63/m
a (Å)	11.483	7.860	9.808	15.901	8.026
b (Å)	14.320	7.860	14.110	6.018	8.026
c (Å)	7.925	5.797	7.816	8.069	6.022
α (°)	90	90	90	90	90
β (°)	90	90	142.38	121.05	90
γ (°)	90	120	90	90	120

Supplementary Figure 5. Proposed crystal structures of $Na_{2+x}C_6O_6$ (**a, b**) and predicted XRD patterns (**c**) in the range of 35º to 50º in the lowest energy reproduced from DFT calculation by Oguchi et al.[17] The interlayer spacing was scaled (max 5%) for each composition based on our experimental XRD results due to the intrinsic limitation of DFT, calculating overestimated Van der Waals force.

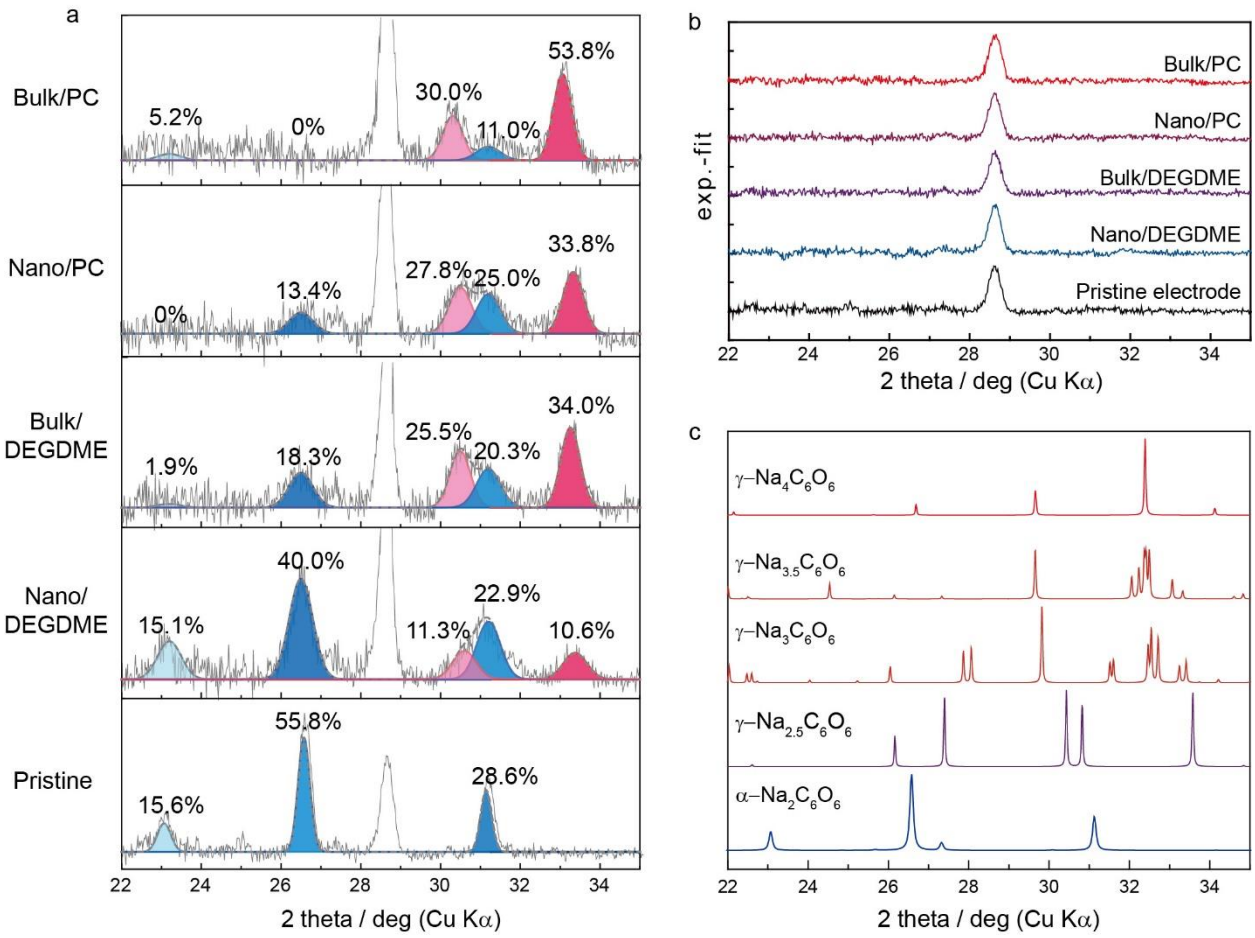

Supplementary Figure 6. **a**, The fit of the diffraction patterns of pristine and cycled electrodes in different conditions using a Gaussian peak-shape function. The areal fraction is calculated for each peak. The three peaks with blue color are originated from α-$Na_2C_6O_6$ and other two peaks with red color are from γ-$Na_{2.5}C_6O_6$. **b**, The deviation of fitting from experimental data for each condition. The negligible deviation was obtained after fitting, and the residual peak is from a protective film. **c**, Predicted XRD patterns of $Na_{2+x}C_6O_6$ in the range of 22º to 35º in the lowest energy reproduced from DFT calculation by Oguchi et al.[17] The interlayer spacing was scaled (max 5%) for each composition based on our experimental XRD results due to the intrinsic limitation of DFT, calculating overestimated Van der Waals force.

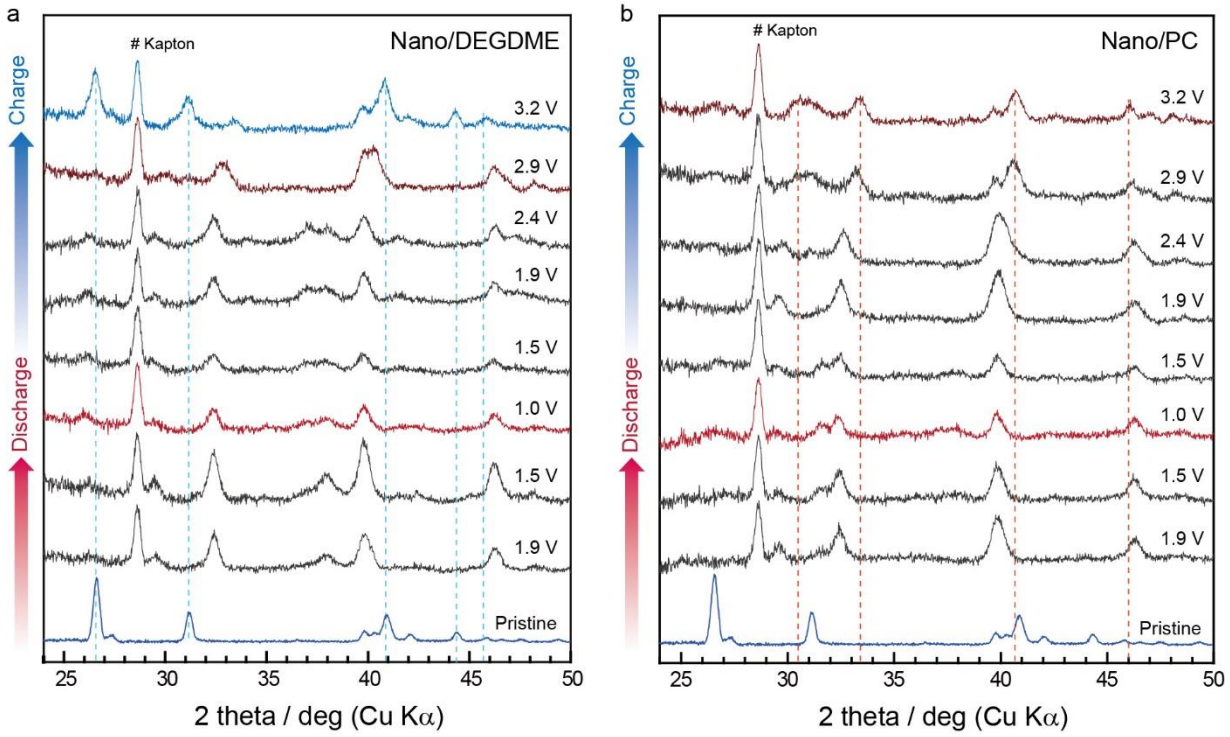

Supplementary Figure 7. *ex situ* XRD spectra of $Na_2C_6O_6$ nanoparticle electrodes at different states of charge during first cycling in (**a**) DEGDME and (**b**) PC.

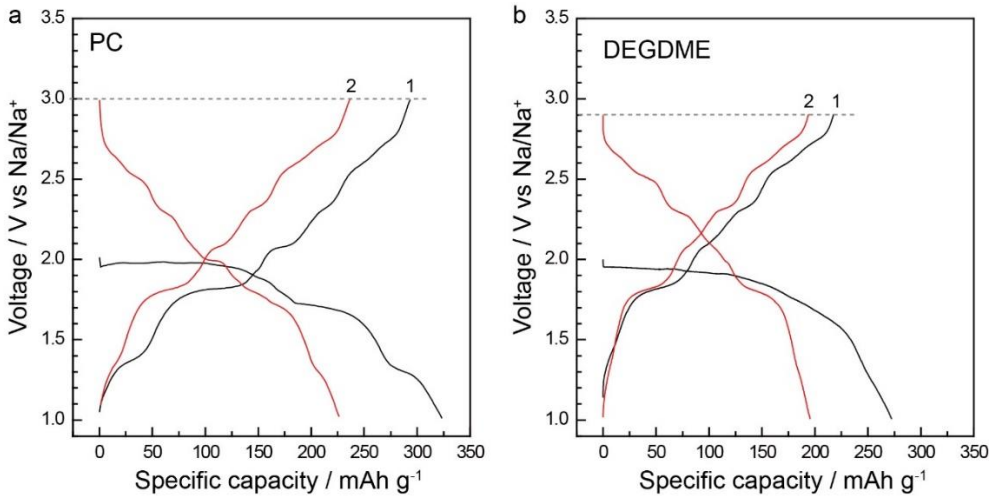

Supplementary Figure 8. Voltage profiles of the first and second cycles with a charge cut off potential at (**a**) 3.0 V in PC, and (**b**) 2.9 V in DEGDME.

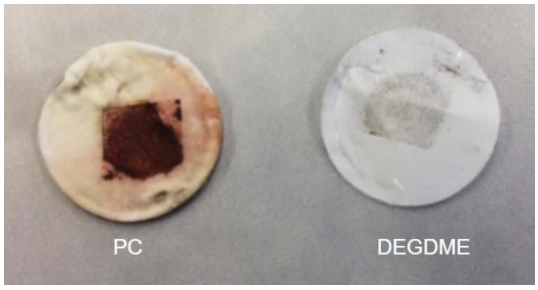

Supplementary Figure 9. A photograph of separators obtained from coin cells after five cycles in 1.0−3.5 V using PC (left), and after 25 cycles in 1.0−3.3 V using DEGDME (right).

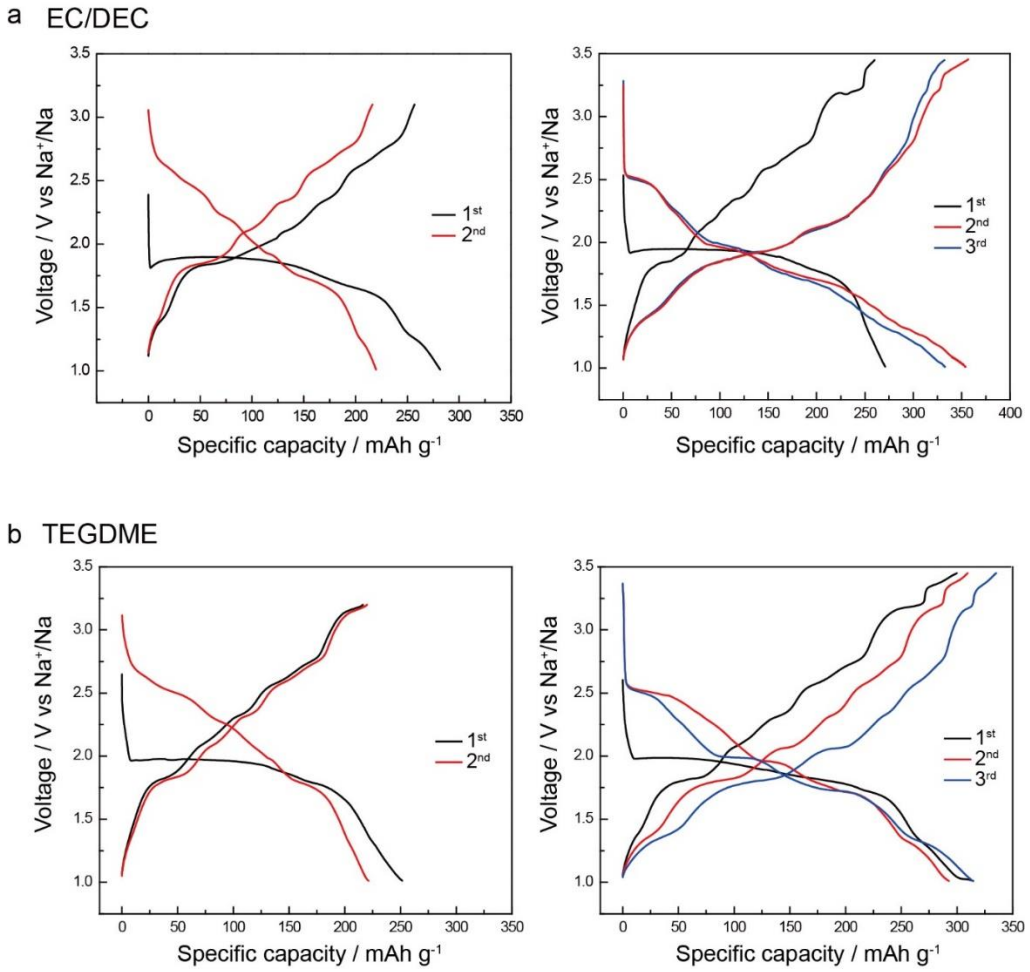

Supplementary Figure 10. Voltage profiles of $Na_2C_6O_6$ nanoparticle electrodes with and without overcharging in 1 M $NaPF_6$ in EC/DEC (**a**) and 0.6 M $NaPF_6$ in TEGDME (**b**).

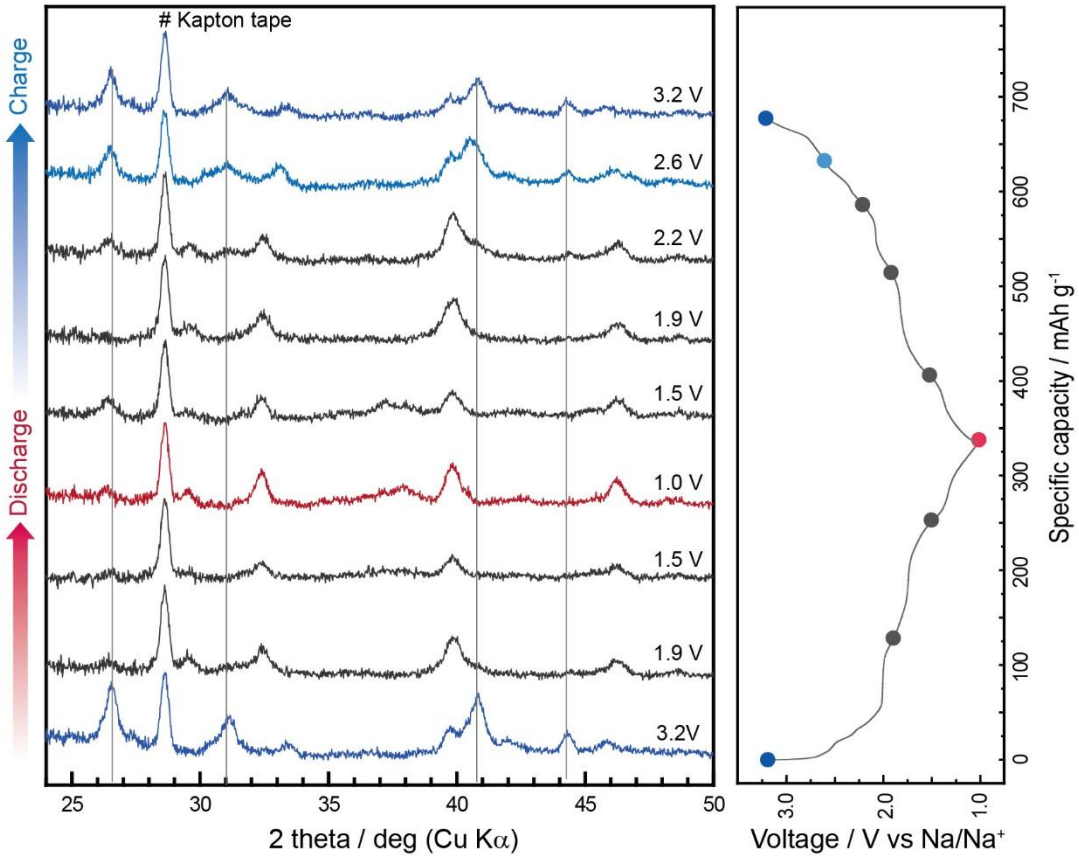

Supplementary Figure 11. *ex situ* XRD results of $Na_2C_6O_6$ nanoparticle electrodes at different states of charge during second cycling in DEGDME.

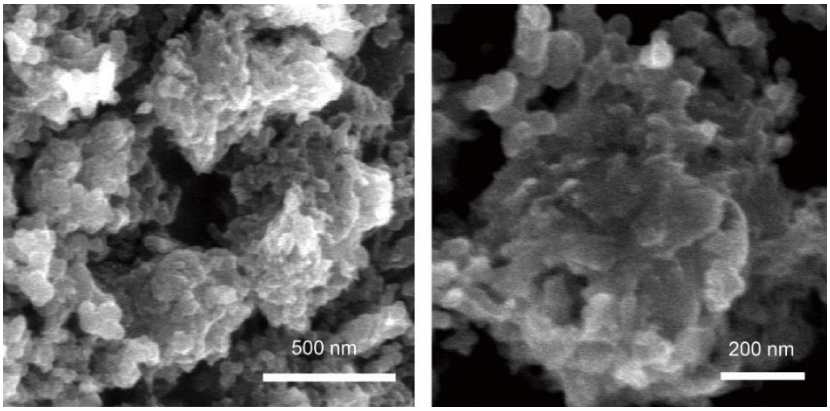

Supplementary Figure 12. *ex situ* SEM images of $Na_2C_6O_6$ nanoparticles after second charge in DEGDME.

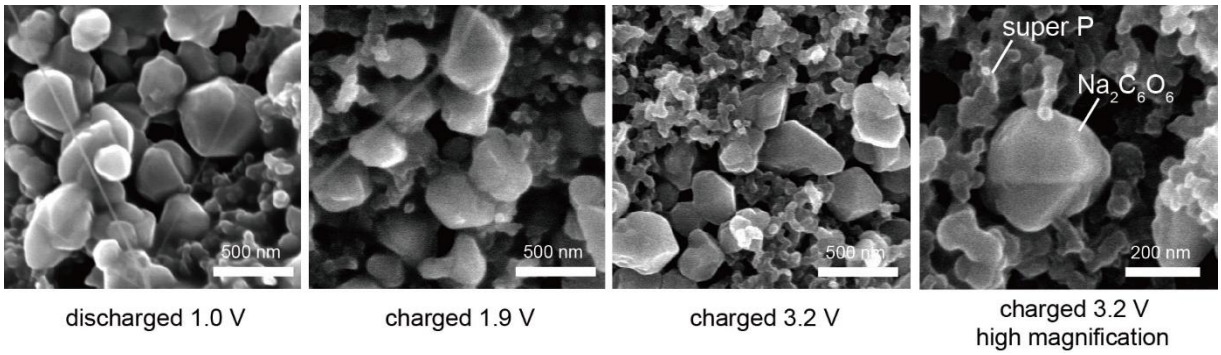

Supplementary Figure 13. *ex situ* SEM images of $Na_2C_6O_6$ nanoparticle electrodes at different states of charge during the first cycle in PC showing negligible change in the particle morphology.

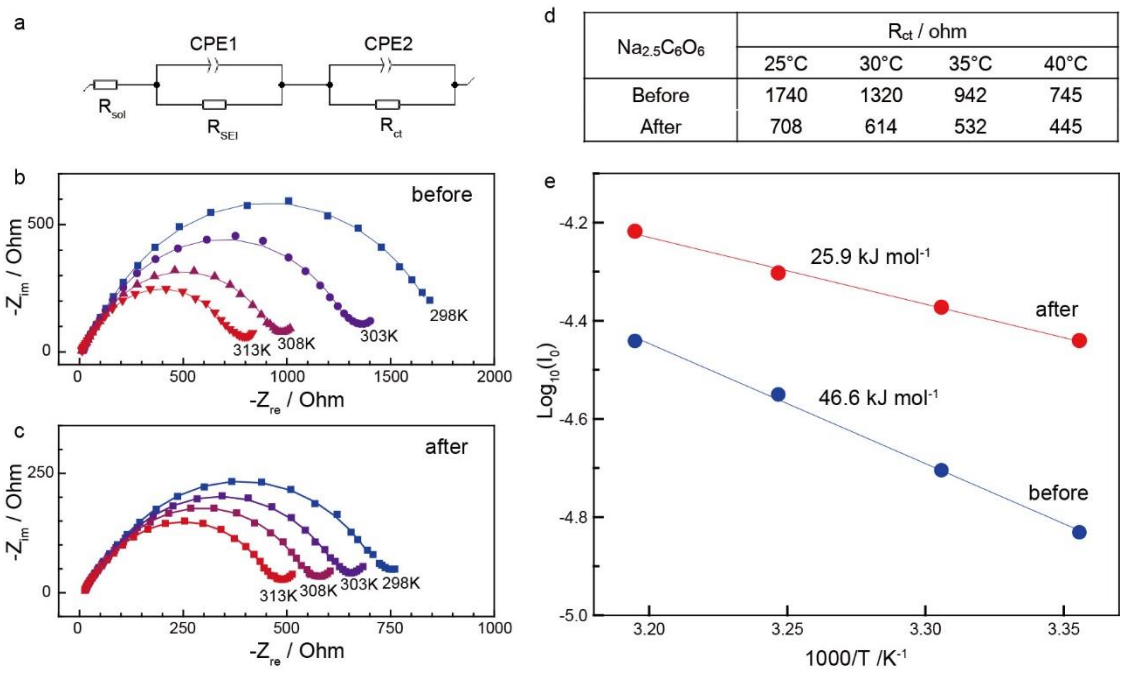

d

$Na_{2.5}C_6O_6$	R_{ct} / ohm			
	25°C	30°C	35°C	40°C
Before	1740	1320	942	745
After	708	614	532	445

Supplementary Figure 14. a-c. Nyquist plots of Nano/DEGDME with the cathode composition of $Na_{2.5}C_6O_6$ before (**b**) and after (**c**) nanostructuring. The solid lines are the fitted curve with the equivalent circuit (**a**). **d.** R_{ct} results at different temperatures from (**b, c**) after fitting. **e**. Arrhenius plots of log i_0 as a function of T^{-1} for $Na_{2.5}C_6O_6$ before and after nanostructuring. The lines are the linear fitting results. The apparent activation energies ($E_a = -RK \ln 10$, where K = the slope of the fitting line) of the sample before and after nanostructuring are calculated to be 46.6 and 25.9 kJ mol^{-1}, respectively.

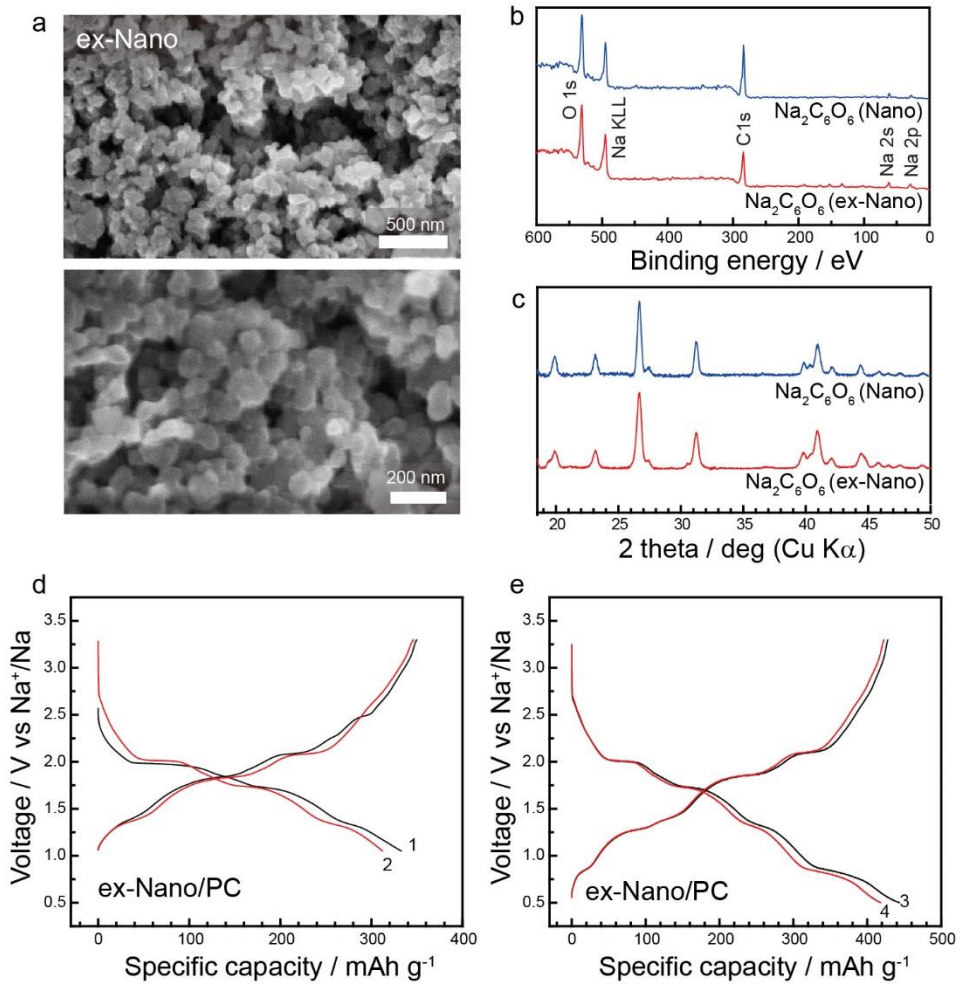

Supplementary Figure 15. a. SEM images of $Na_2C_6O_6$ particles on the order of several tens of nanometers (ex-Nano) prepared through cation exchange from $K_2C_6O_6$. **b,c.** XPS spectra (**b**) and XRD pattern (**c**) of ex-Nano particles in comparison with that of $Na_2C_6O_6$ nanoparticles, confirming that the chemical composition and crystal structure are identical. **d,e.** Voltage profiles of ex-Nano $Na_2C_6O_6$ electrodes in PC electrolyte obtained from a potential window of 1.0-3.2 V during the first and second cycles (**d**), and a potential window of 0.5-3.2 V in the following 3-4 cycles (**e**).

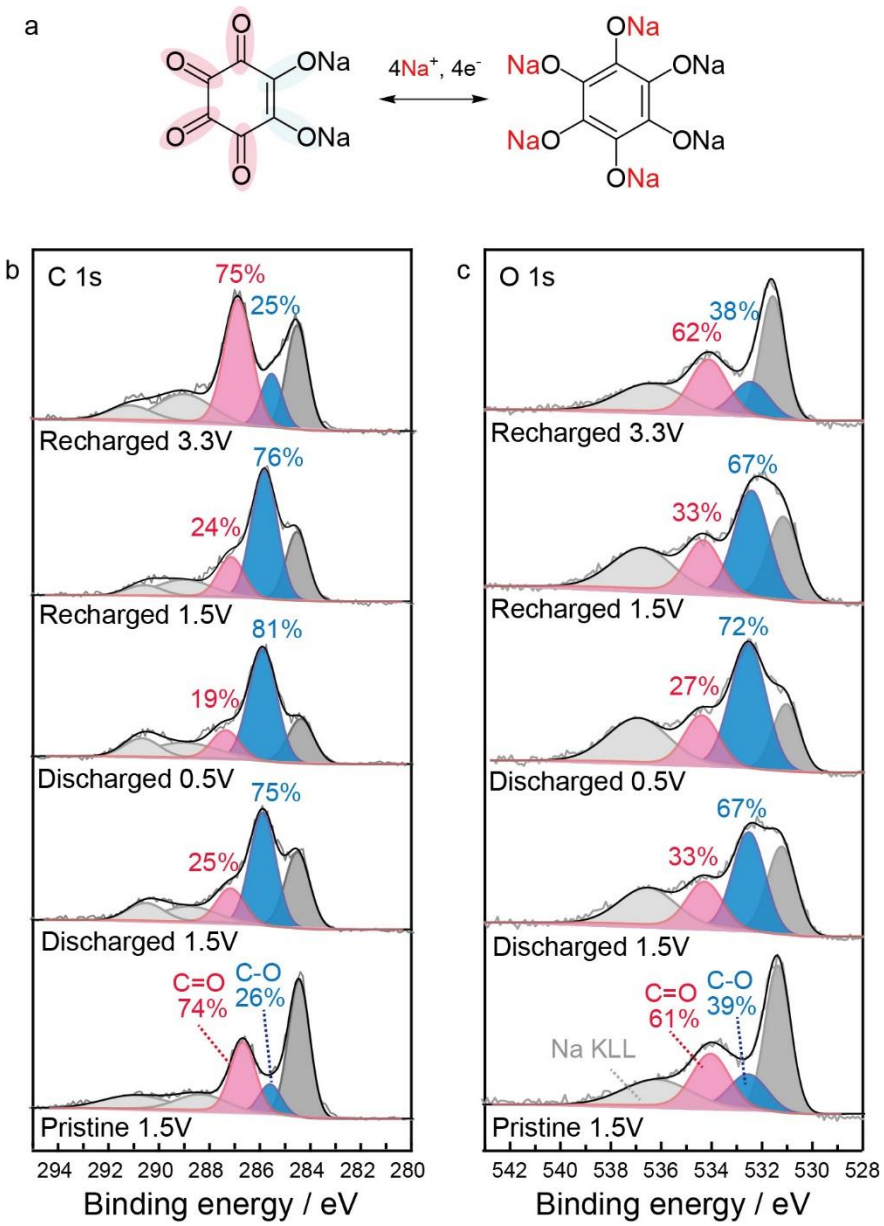

Supplementary Figure 16. **a**. Proposed redox mechanism of $Na_2C_6O_6$ using carbonyl groups as redox active centers. **b,c.** The fit of the XPS spectrum of pristine and cycled electrodes in different states of charge using a Gaussian peak-shape function in the regions of C 1s (**a**), and. O 1s (**b**). The areal fraction is calculated for two peaks, which correspond to C=O and C-O bonds in $Na_2C_6O_6$, respectively. The reversible down-shift of the binding nature in carbon and oxygen atoms in $Na_2C_6O_6$ during the discharge/charge cycle confirms that carbonyl groups act as redox active sites.

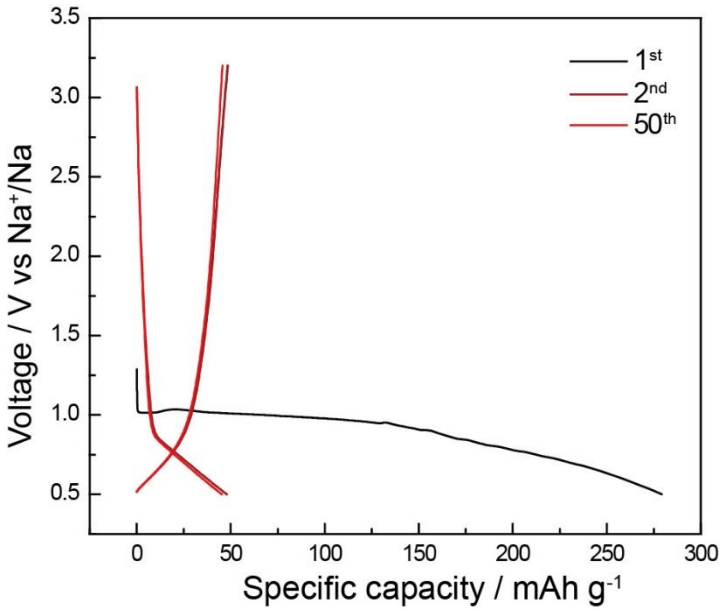

Supplementary Figure 17. Voltage profiles of Super P electrode versus sodium in the voltage range of 0.5- 3.2 V vs Na^+/Na at a current density of 50 mA g^{-1}. Super P exhibits a specific capacity of 47 mAh g^{-1} in the second cycle, and therefore the capacity from 30 wt% of Super P is calculated to be 14 mAh g^{-1}in $Na_2C_6O_6$ electrode.

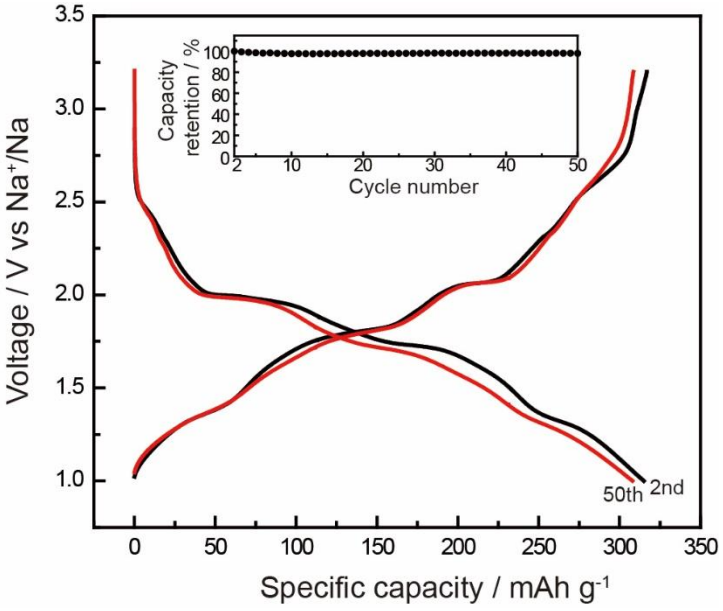

Supplementary Figure 18. Capacity retention of a nanoparticle electrode in DEGDME in a small potential window of 1.0 to 3.2 V at 100 mA g^{-1}.

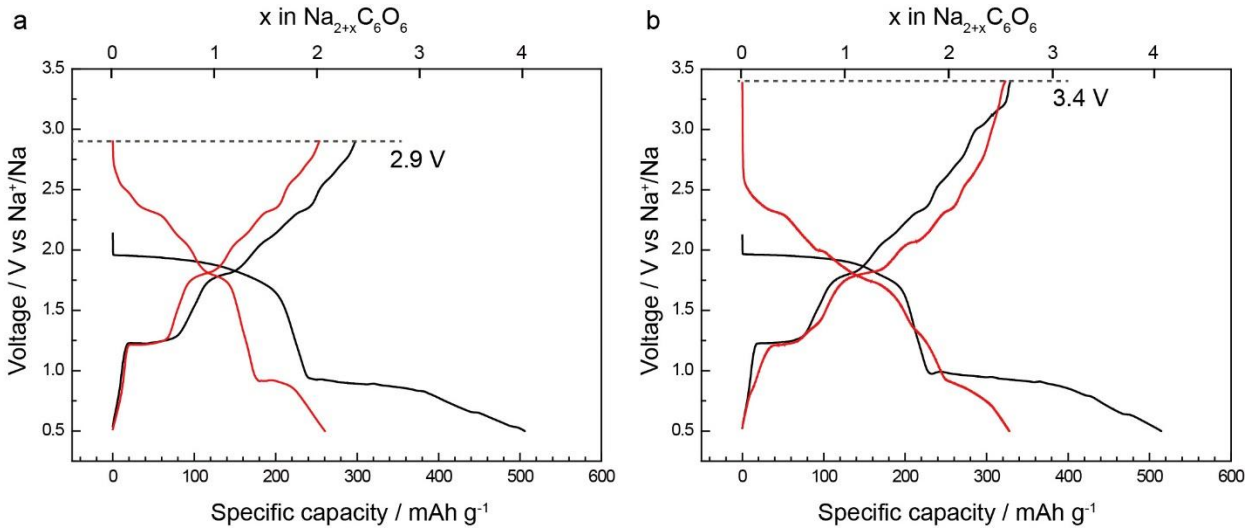

Supplementary Figure 19. Electrochemical performances of $Na_2C_6O_6$ bulk electrodes with discharge cut-off potential of 0.5 V, and with charge cut-off potential of 2.9 V (**a**), and 3.4 V (**b**).

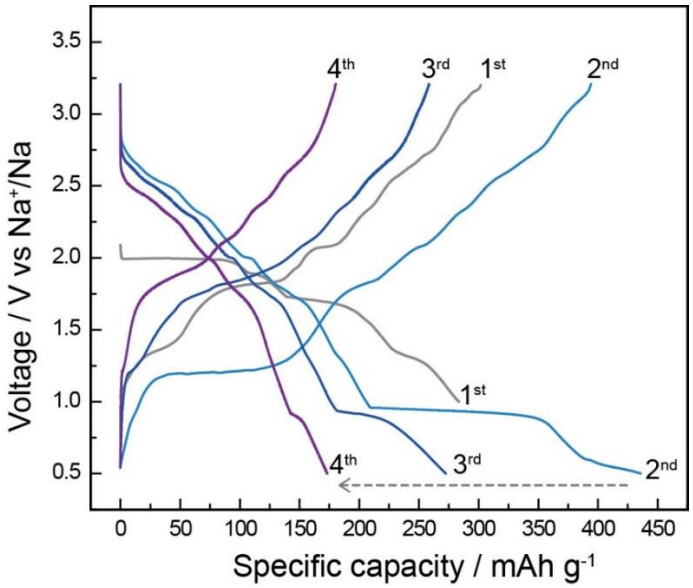

Supplementary Figure 20. Voltage profiles of $Na_2C_6O_6$ nanoparticle electrode in PC obtained from a wide potential window of 0.5-3.2 V, except for the first cycle in a potential window of 1.0-3.2 V.

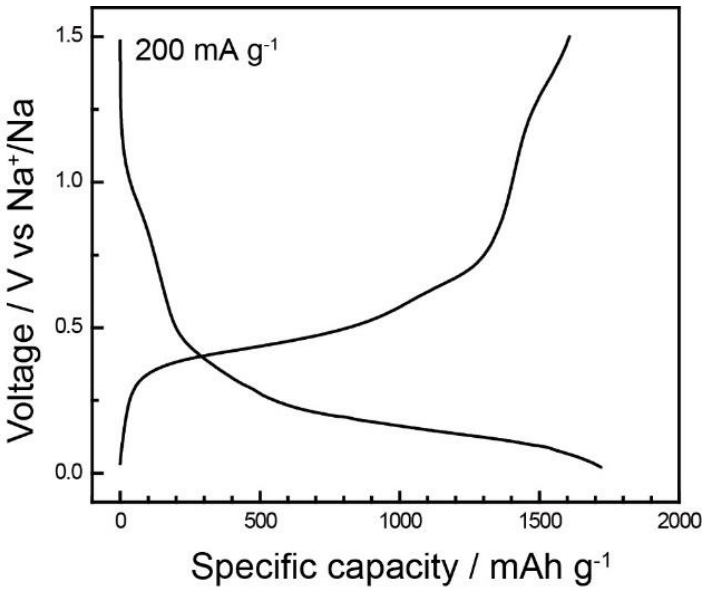

Supplementary Figure 21. A typical voltage profile of a red phosphorous (red P) electrode (red P : porous carbon : PVDF = 40 : 50 : 10) in a half cell versus sodium using 0.6 M $NaPF_6$ in DEGDME. The theoretical capacity is to be 2595 mAh g^{-1} based on a reaction, $3Na + P \rightarrow Na_3P$.

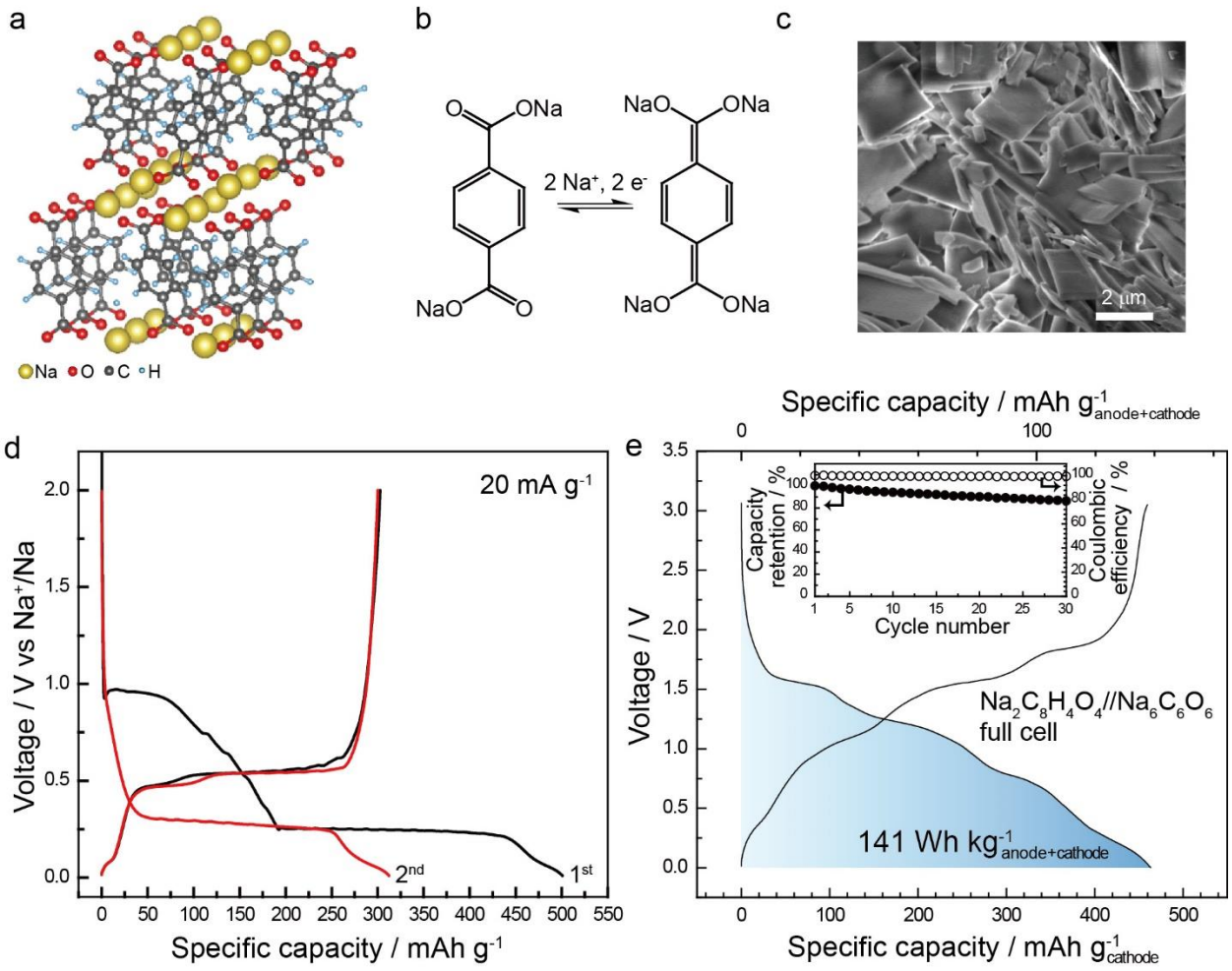

Supplementary Figure 22. a, Crystal structure of $Na_2C_8H_4O_4$, **b**, Molecular structure and sodiation/desodiation mechanism of $Na_2C_8H_4O_4$, **c,** SEM image of pristine $Na_2C_8H_4O_4$ powder, **d**, Voltage profiles of the first and second discharge-charge cycles of $Na_2C_8H_4O_4$ electrode in a half cell versus sodium, **e,** Full cell performance of $Na_2C_8H_4O_4$//$Na_6C_6O_6$ at 50 mA g^{-1}.

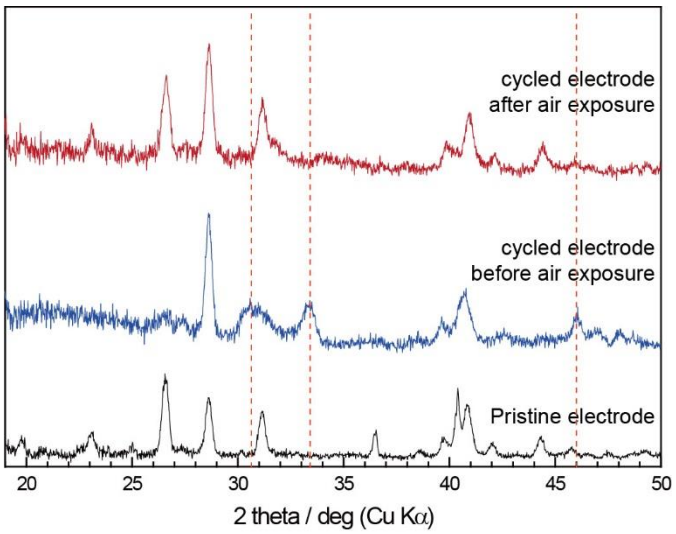

Supplementary Figure 23. XRD patterns of pristine and cycled electrodes in PC before and after air exposure. Once exposed to air, the characteristic peaks from the residual λ phase (red dotted lines) disappeared and the characteristic peaks from the original α phase reappeared in the cycled electrode, indicating air instability of the λ phase.

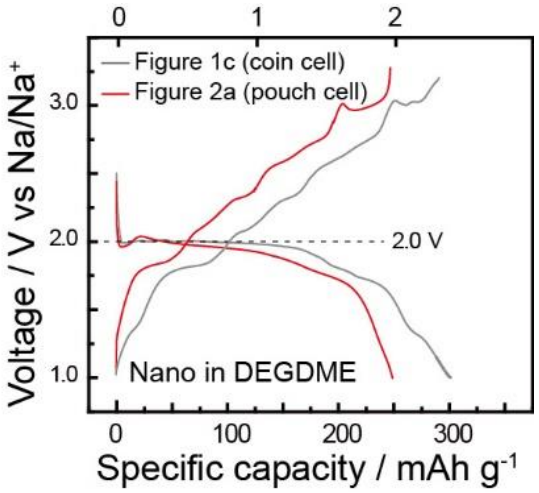

Supplementary Figure 24. Comparison of the first discharge/charge profiles in a coin cell (Figure 2c) and a pouch cell (Figure 2a). The slight deviation in the operating potential and capacity is due to the higher impedance in the pouch cell than that in the coin cell.

Supplementary Table

Supplementary Table 1. Sodium storage properties of reported Na full cells[1-4] in comparison with our results.

reference	Anode//Cathode	Mass ratio of cathode/anode	Current density	Capacity	Energy density
our work	P@C//$Na_6C_6O_6$	3.8	50 mA/$g_{cathode}$	264 mAh/$g_{anode+cathode}$	281 Wh/$kg_{anode+cathode}$
our work	$Na_2C_8H_4O_4$//$Na_6C_6O_6$	0.7	50 mA/$g_{cathode}$	137 mAh/$g_{anode+cathode}$	141 Wh/$kg_{anode+cathode}$
[1]	P2-$Na_{0.66}Ni_{0.17}Co_{0.17}Ti_{0.66}O_2$ (symmetric)	2.0-2.2	20 mA/$g_{cathode}$	92 mAh/$g_{cathode}$	95 Wh/$kg_{anode+cathode}$
[2]	nanostructured $Na_2Ti_3O_7$//$VOPO_4$	2.0	10 mA/$g_{cathode}$	76 mAh/$g_{anode+cathode}$	220 Wh/$kg_{anode+cathode}$
[3]	P2-$Na_{0.6}[Cr_{0.6}Ti_{0.4}]O_2$ (symmetric)	0.71-0.88	10 mA/$g_{cathode}$	80 mAh/g_{anode}	94 Wh/$kg_{anode+cathode}$
[4]	$Na_4C_8H_2O_6$ (symmetric)	-	19 mA/$g_{cathode}$	198 mAh/g_{anode}	195 Wh/$kg_{anode+cathode}$

Supplementary Notes

Supplementary Note 1.

The change in discharge curves (Figure 1c, Bulk/PC) can be explained with different origins such as drastic textural modifications,[5] or a change in reaction paths during cycling due to limited reversibility.[6] What we observed in the bulk electrode after cycling was slight crack formation for some particles while overall the original shape was maintained after the sodiation/desodiation process (Supplementary Figure 3). This is not as dramatic as the morphology change of transition metal oxides during conversion reactions which show similar voltage hysteresis.[5,7] Also, if the first discharge process is kinetically limited and facilitated with textural modifications during cycling, as previous study assumed,[8] then the large polarization should also be mitigated by decreasing the rate of charge, reducing electrode thickness, or minimizing particle-size. But, from the $Na_2C_6O_6$ electrode with a reduced particle size from several tens of micrometers to several hundreds of nanometers (Figure 1b), we still observed the identical plateau at 2.0 V in the first discharge and the evolution of discharge profile with a decreased capacity in the following cycles (Figure 1c, Nano/PC). The only notable change was that the redox potential below 1.9 V is more accessible in nanoparticles than bulk particles in the first cycle.

Supplementary Note 2.

We conducted X-ray photoelectron spectroscopy (XPS) analysis to probe evolution of redox active sites in $Na_2C_6O_6$ upon cycling (Supplementary Figure 18). An air-tight transfer vessel allowed us to protect the electrodes retrieved from cycled Na cells for the XPS analyses. During the discharge/charge cycle, the reversible shifts to lower binding energy in carbon and oxygen atoms were observed in $Na_2C_6O_6$. The C 1s XPS spectrum from pristine electrode shows two predominant peaks at 285.5 and 286.8 eV, which are attributed to the C–O, and C=O bonds in $Na_2C_6O_6$, respectively. The other peaks are associated with C–C/C–H and C–F bonds from conductive carbon and binder in the composite electrode. According to the fit of C 1s spectrum at different states of charge during cycling, the areal fraction calculated for C=O bonds verses C–O bonds gradually decreases and recovers. This phenomenon is consistent with the changes in the O 1s XPS spectrum, where the peak at 534.1 eV assigned to the C=O bonds shifts to lower energy and recovers. This suggests that electron density of C and O atoms increases during discharge which results in lower binding energy in both atoms compared to the pristine state. Such change is fully reversible upon charge as confirmed with the recovery of the original areal fraction of C=O bonds versus C–O bonds in C 1s and O1s from the electrode recharged to 3.3 V. Therefore, we concluded that carbonyl groups work as the redox active sites in $Na_2C_6O_6$.

Supplementary References

1 Guo, S. *et al.* A High-Voltage and Ultralong-Life Sodium Full Cell for Stationary Energy Storage. *Angewandte Chemie International Edition* **54**, 11701-11705, (2015).

2 Li, H. *et al.* An advanced high-energy sodium ion full battery based on nanostructured Na2Ti3O7/VOPO4 layered materials. *Energy & Environmental Science* **9**, 3399-3405, (2016).

3 Wang, Y., Xiao, R., Hu, Y.-S., Avdeev, M. & Chen, L. P2-Na0.6[Cr0.6Ti0.4]O2 cation-disordered electrode for high-rate symmetric rechargeable sodium-ion batteries. *Nature Communications* **6**, 6954, (2015).

4 Wang, S. *et al.* All Organic Sodium-Ion Batteries with Na4C8H2O6. *Angewandte Chemie International Edition* **53**, 5892-5896, (2014).

5 Poizot, P., Laruelle, S., Grugeon, S., Dupont, L. & Tarascon, J. M. Nano-sized transition-metal oxides as negative-electrode materials for lithium-ion batteries. *Nature* **407**, 496-499, (2000).

6 Kim, H. *et al.* Understanding Origin of Voltage Hysteresis in Conversion Reaction for Na Rechargeable Batteries: The Case of Cobalt Oxides. *Advanced Functional Materials* **26**, 5042-5050, (2016).

7 Xu, K., Lam, Y., Zhang, S. S., Jow, T. R. & Curtis, T. B. Solvation Sheath of Li+ in Nonaqueous Electrolytes and Its Implication of Graphite/Electrolyte Interface Chemistry. *The Journal of Physical Chemistry C* **111**, 7411-7421, (2007).

8 Wang, C. *et al.* Manipulation of Disodium Rhodizonate: Factors for Fast-Charge and Fast-Discharge Sodium-Ion Batteries with Long-Term Cyclability. *Advanced Functional Materials* **26**, 1777-1786, (2016).